

Motility Modulates the Partitioning of Bacteria in Aqueous Two-Phase Systems

Jiyong Cheon,^{1,*} Kyu Hwan Choi,^{2,*} Kevin J. Modica,²
Robert J. Mitchell,³ Sho C. Takatori,^{2,†} and Joonwoo Jeong^{1,‡}

¹Department of Physics, Ulsan National Institute of Science and Technology, Ulsan, Republic of Korea

²Department of Chemical Engineering, University of California, Santa Barbara, Santa Barbara, CA, USA

³Department of Biological Sciences, Ulsan National Institute of Science and Technology, Ulsan, Republic of Korea

(Dated: May 16, 2024)

We study the partitioning of motile bacteria into different thermodynamic states of a phase-separated dextran (DEX)/polyethylene glycol (PEG) aqueous mixture. While non-motile bacteria partition exclusively into the DEX-rich phase in all conditions tested, we observed that motile bacteria transverse the soft DEX/PEG interface and partition variably among the two phases. For our model organism *Bacillus subtilis*, the fraction of motile bacteria in the DEX-rich phase increased from 0.58 to 1 as we increased DEX composition within the two-phase region. We hypothesized that the chemical affinity between dextran and the bacteria cell wall acts to weakly confine the bacteria within the DEX-rich phase; however, motility can generate sufficient mechanical forces to overcome the soft confinement and propel the bacteria into the PEG-rich phase. Using optical tweezers to drag a bacterium across the DEX/PEG interface, we developed a model to predict the overall phase partitioning based on a competition between the interfacial forces and bacterial propulsive forces. Our measurements are supported by a theoretical model of dilute active rods embedded within a periodic soft confinement potential.

The behavior of living bacteria in multiphase aqueous suspensions plays an important role in many biological and ecological systems, such as in infection routes and cell sorting [1–3]. Prior work has shown that living bacteria immersed in an aqueous two-phase system (ATPS) of dextran (DEX) and polyethylene glycol (PEG) eventually partition into one phase [4–9]. However, the basic mechanisms underlying the biased partitioning of living bacteria into different phases of ATPS mixtures, especially in the presence of bacteria motility, remain unknown.

For systems at thermodynamic equilibrium, passive colloidal particles immersed in a DEX/PEG mixture have been shown to partition into different bulk phases depending on the surface properties of the colloids [10–13]. By coating the colloidal surfaces with different chemical moieties, the partitioning of passive colloids into the DEX-rich versus PEG-rich phases follows the equilibrium-based Boltzmann distribution, $P(\mathbf{x}) \propto \exp(-V(\mathbf{x})/(k_B T))$, where $V(\mathbf{x})$ describes the interaction energy landscape of the particle in the mixture [13–15]. In contrast, the partitioning of motile bacteria in two-phase systems is not guaranteed to obey Boltzmann statistics because the bacteria generate nonequilibrium forces through their motility.

In this Letter, we combine experiment and theory to study the partitioning of motile bacteria in a DEX/PEG system using *Bacillus subtilis* as a model organism. As shown in Fig. 1A-B, we confined the bacteria into a quasi-2D system immersed in a phase-separated mixture of PEG-rich domains surrounded by DEX-rich phase. We observed that non-motile *B. subtilis* only exhibited Brownian motion and partitioned entirely into the DEX-rich phase (Fig. 1C). In contrast, motile *B. subtilis* dis-

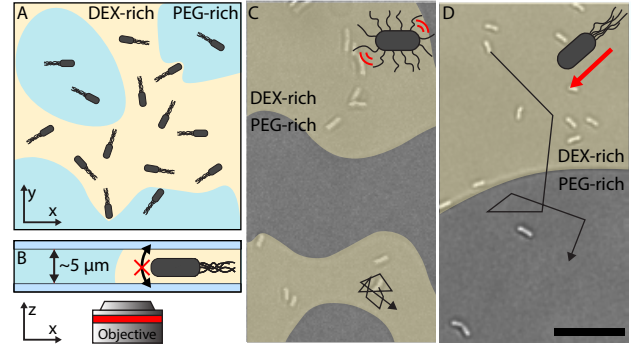


FIG. 1. Motile bacteria *B. subtilis* immersed in an aqueous two-phase system (ATPS) of dextran (DEX) and polyethylene glycol (PEG) partition more evenly across the two phases compared to non-motile ones, which partition exclusively into the DEX-rich phase. A) Top and B) side views of our quasi-2D setup for measuring bacterial partitioning. The chamber thickness is $5\mu\text{m}$ to prevent the bacteria (average body length $\approx 5\mu\text{m}$) from orienting vertically. C) Non-motile *B. subtilis* partition exclusively into the DEX-rich phase (yellow region), whereas the D) motile ones partition into both phases. Total concentrations of DEX and PEG are 3.2 and 2.5 wt/wt%, respectively. The scale bar is $20\mu\text{m}$.

tributed more evenly across the two phases and reached a dynamic steady-state, with bacterial cells frequently crossing the DEX/PEG interface (Fig. 1D; see also Movie S1). We also observed an asymmetric interfacial deformation by bacteria transverse the two-phase boundary, always toward the DEX-rich phase: when crossing from DEX \rightarrow PEG, we observed the interface bend outwards away from the bacterium, generating an antiparallel force against bacterial swimming. In contrast, when crossing from PEG \rightarrow DEX, we observed the interface bend inwards towards the bacteria, generating a parallel force aligned with swimming. Based on these observa-

tions, we hypothesized that chemical affinities between dextran sugars and components on the *B. subtilis* cell wall (such as other sugars) act to weakly confine the bacterium within the DEX-rich phase; however, motility can generate sufficient mechanical forces to overcome this ‘soft’ confinement and propel the bacterium into the PEG-rich phase. If true, we further hypothesize a dynamic steady-state between these two forces should lead to partitioning ratios of motile bacteria between the two phases.

To quantify our bacterial partitioning observations, we defined the partitioning ratio as the number of bacteria in the DEX-rich phase divided by the total number of bacteria in the sampled area (see Supplemental Figs. S2 and S3). As shown in Fig. 2, non-motile *B. subtilis* has a partitioning ratio of 1 across all DEX concentrations tested (1.5 - 8.0 wt/wt%) with a fixed PEG concentration (2.5 wt/wt%). In contrast, the partitioning ratio for the motile bacteria increased monotonically from 0.58 ± 0.10 at 1.5 wt/wt% DEX concentration, to 1.00 at 8.0 wt/wt%.

Several possible mechanisms of biased partitioning of motile bacteria may explain our results, including motility, chemical gradient, and chemical affinity. One possible mechanism is based on the difference in viscosities of the PEG-rich and DEX-rich phases. A larger drag in the DEX-rich phase may slow down the bacterium, leading to its accumulation in the DEX-rich phase from an effect analogous to motility-induced phase separation (MIPS) of active Brownian particles [16–18]. In a control experiment, we measured the *B. subtilis* swimming speeds in the DEX-rich phase ($30.7 \pm 6.1 \mu\text{m/s}$) and in the PEG-rich phase ($34.5 \pm 6.4 \mu\text{m/s}$) at 3.2 wt/wt% dextran concentration. Variable swimming speeds would produce a density distribution as $n(x) \sim 1/U(x)$, and we expect the $\approx 10\%$ slower speeds in the DEX-rich phase to give a partitioning ratio, $n_{\text{DEX}}/(n_{\text{DEX}} + n_{\text{PEG}}) = (1 + U_{\text{DEX}}/U_{\text{PEG}})^{-1} \approx 0.52$. This, however, does not fully explain the partitioning observed in our experiments for the same condition, 0.78 ± 0.08 (Fig. 2). Another possible mechanism is bacterial sensing of chemical attractants, such as glucose, through chemotaxis. *B. subtilis* is attracted by sugar (glucose) gradients [19]. Upon imaging the DEX-PEG interface using dextran-FITC (see Supplemental Fig. S4), we observed a sharp gradient of dextran near the interface over a narrow width of $\approx 2 \mu\text{m}$, surrounded by a constant dextran concentration in the bulk phases outside of this narrow interface. Since chemotaxis requires chemical gradients to persist over distances larger than the run length ($\gg 100 \mu\text{m}$) and the body length of an individual bacterium ($\approx 5 \mu\text{m}$) [20], chemotaxis is unlikely to explain the biased partitioning of motile bacteria noted in our experiments.

As an alternative mechanism to explain our results, we hypothesized that the chemical affinity between the DEX-rich phase and the chemical components on the

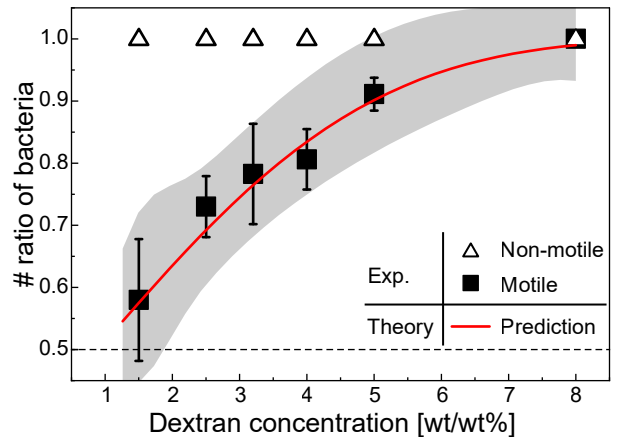


FIG. 2. Experimental and predicted partitioning ratios of bacteria in DEX-rich phase versus dextran concentration of the overall mixture, where open and filled symbols are experimental results of non-motile and motile bacteria, respectively, and the red solid curve is the predicted partitioning ratio based on our theory, Eqs. 1 and 2. The shaded region represents the 95% confidence band of our model. The horizontal dash line at 0.5 represents a theoretical partitioning ratio when the two-phase boundary vanishes at the critical composition.

bacterial cell wall drives the partitioning. Toward this end, we performed optical tweezer experiments to drag single bacterial cells across the DEX-PEG interface and measured the forces required for this bacterium to cross the two-phase boundary (Fig. 3A). We attached a tracer silica bead as a calibration handle to the bacteria cell wall using click chemistry (See Fig. 3A, Supplemental Figs. S5 and Movie S2). We used silica beads because precise forces are easier to compute on trapped spherical particles, and because the bead can sit at the DEX-PEG boundary without creating additional interfacial deformations. We translated the trap location from the DEX-rich phase into the PEG-rich phase at sufficiently small speeds (0.5 or $2 \mu\text{m/s}$) to ignore the viscous drag force on the bead. Using the displacement of the bead center from the trap center, we measured the force generated by the two-phase boundary on the bacterium, F_{int} , as shown in Fig. 3B, while Supplemental Fig. S5 describes these interactions.

First, consistent with our initial observations of interface deformation as the bacterial cell crossed the boundary, we observed the interface always applies a force on *B. subtilis* towards the DEX-rich phase. As the bacterial body crossed the interface from DEX-rich to PEG-rich phases, the interface deformed and pulled the bacterium back towards the DEX-rich phase, causing the magnitude of the net force to increase as a function of distance. When the magnitude of F_{int} reached a maximum, F_{max} , the interface slipped along the surface of the bacterium until the bacterium completely penetrated and crossed the interface. Then, the interface recovered its initial unperturbed shape. At this point where the bacterium was

now submerged completely inside the PEG-rich phase, F_{int} suddenly released to zero.

We conducted the measurement across several different dextran compositions in the APTS mixture. As shown in Fig. 3C, F_{max} has magnitudes $\sim \mathcal{O}(\text{pN})$ and increases with dextran concentration. These force measurements are direct reporters of the force experienced by swimming bacteria as they cross the interface from the DEX-rich to PEG-rich phases. Our measurements corroborate our hypothesis that thermal forces alone are not sufficient to allow non-motile bacteria to cross the two-phase boundary ($1k_{\text{B}}T/1\mu\text{m} \approx 10^{-3}\text{pN} \ll \mathcal{O}(\text{pN})$). Therefore, in the absence of a propulsion force, all our non-motile *B. subtilis* partitioned into the DEX-rich phase across all conditions tested in Fig. 2. In contrast, for motile bacteria, propulsion forces of magnitude $F_{\text{prop}} \sim \mathcal{O}(\text{pN})$ is sufficiently large to overcome the maximum forces generated by the interface, F_{max} . For lower dextran concentrations, where F_{max} is smaller (see Fig. 3C), the propulsion forces have an even larger success of bacteria barrier crossing. Correspondingly, the partitioning ratio is more even between the two phases for the lower dextran concentrations, as shown in Fig. 2. For the largest dextran concentration test, 8.0 wt/wt%, the interfacial forces (F_{int}) are too strong for the laser trap to drag the bacteria completely inside the PEG-rich phase. Namely, the laser trap lost the handle bead prior to crossing the interface, and we were unable to measure F_{max} since F_{max} is greater than the maximum force that the trap could exert on the bead. Consistent with this observation, the motile *B. subtilis* partitioned completely inside the DEX-rich phase at a 8.0 wt/wt% dextran concentration, likely because the propulsion forces were always smaller than the interfacial barrier, $F_{\text{prop}} < F_{\text{max}}$ (See Movie S3).

To corroborate our experimental measurements, we modeled the affinity of the bacteria to the DEX-rich phase as an external field which drives the bacteria to regions of high dextran concentration. We then developed an active Brownian particle model that predicts the partitioning of self-propelled particles subject to that potential driving force. The Smoluchowski equation describing the evolution of probability for a dilute system of swimming rod-like particles in a potential field is given by [21, 22]

$$\frac{\partial P}{\partial t} + \frac{\partial}{\partial x} \left[\frac{P}{\zeta} \left(F_{\text{prop}} \cos \theta - k_{\text{B}}T \frac{\partial \ln P}{\partial x} - \frac{\partial V}{\partial x} \right) \right] + \frac{\partial}{\partial \theta} \left[P \left(-\frac{1}{\tau_{\text{R}}} \frac{\partial \ln P}{\partial \theta} - \frac{1}{\zeta_{\text{R}}} \frac{\partial V}{\partial \theta} \right) \right] = 0, \quad (1)$$

where x and θ are the position and orientation of the active particle, ζ and ζ_{R} are translational and rotational drag coefficients, F_{prop} is the propulsion force, τ_{R} is the reorientation time, and $V(x, \theta)$ encodes the energetic cost for the bacterium to move from the DEX-rich phase to the PEG-rich phase (see Supplementary Infor-

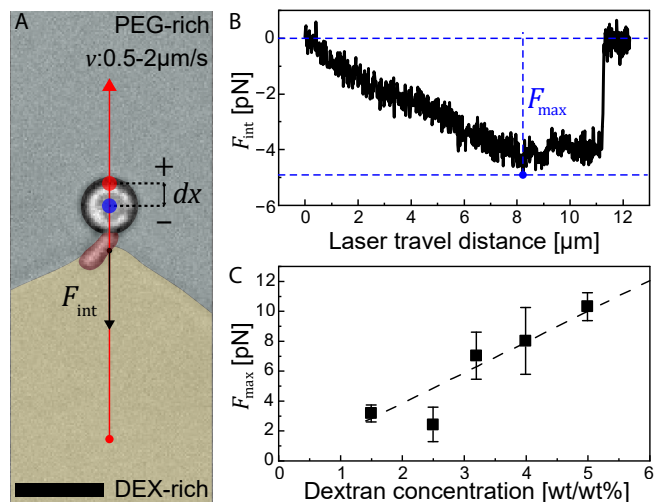


FIG. 3. Optical tweezers were used to drag a single bacterium across the two-phase boundary and measure the forces imparted on the bacterium. A) Representative snapshot of a bacterium attached to a tracer bead crossing the interface. The red solid arrow is the path of the optical trap. The force generated by the interface, F_{int} , is calculated by measuring the displacement, dx , between the laser focal point (red dot) and the tracer bead center (blue dot). Negative values indicate the force is directed against the movement. The scale bar is $5 \mu\text{m}$. B) Representative force profile of F_{int} as the bacterium crosses the two-phase boundary. The laser travel distance is set to zero when the bacterium-bead assembly experiences zero interfacial force. C) Maximum forces (F_{max}) for various dextran concentrations tested. The dashed line represents a linear regression for parameter estimation in our theory, Eq. 1.

mation for the functional form). Assuming the bacterium is a thin rod, we can relate their rotational and translational drag coefficients using the length of the bacterium $\zeta/\zeta_{\text{R}} = 6/\ell_{\text{bact}}$. For simplicity we ignore the orientation dependence on the translational drag coefficient, and treat the PEG-rich and DEX-rich phases as a 1-D lamellar system with equal domain width $L/2$ in a periodic system of size L . This model can be described with five parameters: the ratio of the maximum interface restoring force to the propulsion force $F_{\text{max}}/F_{\text{prop}}$, the propulsion force relative to the thermal energy ($F_{\text{prop}}L/k_{\text{B}}T$), the thermal diffusivity relative to the reorientation time ($L^2\zeta)/(\tau_{\text{R}}k_{\text{B}}T)$, the scaled bacteria length ℓ_{bact}/L , and the scaled interface width δ/L . δ is the length-scale over which the phase transitions from pure PEG-rich to pure DEX-rich. We allow the reorientation time τ_{R} to be determined independently from the drag to account for non-thermal reorientation mechanisms.

Based on this theoretical model, we solved the steady-state Smoluchowski equation assuming the bacteria are thin rods, using the methods described in recent work [21]. The partitioning ratio is determined by the fraction

of bacteria in the DEX-rich phase:

$$\frac{n_{\text{DEX}}}{n_{\text{DEX}} + n_{\text{PEG}}} = \int_0^{2\pi} \int_{-L/4}^{L/4} P(x, \theta) dx d\theta \quad (2)$$

We integrated between $\pm L/4$ because that is the energetically favorable DEX-rich phase, and the rest of the domain is the PEG-rich phase. Based on the average measured propulsive force of $F_{\text{prop}} \approx 10\text{pN}$ (See Supplemental Fig. S6C, [23]), we used a linear regression to relate the dextran concentration to the maximum restoring force (see Fig. 3C) to determine the force ratio, $F_{\text{max}}/F_{\text{prop}}$. Due to a large parameter space, we used the experimentally determined propulsion force and bacteria length to set $(F_{\text{prop}}L)/k_{\text{B}}T = 5 \times 10^5$ and $\ell_{\text{bact}}/L = 0.025$. We found the remaining parameters (δ/L and $(L^2\zeta)/(\tau_R k_{\text{B}}T)$) using a nonlinear-least-squares regression, while bounding them to be within a realistic range based on the experimental system. Due to the order of magnitude difference in parameter values, the regression was performed on their logarithms and converged to $\log_{10}[(L^2\zeta)/(\tau_R k_{\text{B}}T)] = 8.0 \pm 2.0$ and $\log_{10}[\delta/L] = -2.6 \pm 1.8$.

As shown in Fig. 2, our model is able to predict the increased partitioning as the maximum restoring force grows (dextran concentration is obtained from F_{max} by the regression in Fig. 3C). Similar to the experimental trend observed with motile bacteria, the prediction line also increases monotonically with dextran concentration from 0.57 ± 0.14 at 1.5 wt/wt% to 0.99 ± 0.07 at 8.0 wt/wt%, corresponding to experimental ratios of 0.58 ± 0.10 and 1.00 respectively. As the energy barrier (and F_{max}) grows, it becomes difficult for this bacterium to escape across the interface using their propulsion force alone. At a steady state, this results in more bacteria being trapped in the low energy region, *i.e.*, DEX-rich phase, until they make a statistically unlikely Brownian move into the PEG-rich region. In contrast, when the energy barrier is weak, the motile bacteria easily penetrate the interface and evenly distribute over the two phases.

The solution to the Smoluchowski equation is the steady-state probability density of dilute active rods as a function of position and orientation. When we integrate the distribution to get the partitioning ratio, we lose a lot of the fine-grain details. As such, there are multiple sets of parameters that give identical partitioning. In our case the parameters $(L^2\zeta)/(\tau_R k_{\text{B}}T)$ and δ/L are strongly anti-correlated, with correlation coefficients nearing -0.99 . We expect this is the primary cause for the large uncertainty in the parameter estimation. Deconvoluting the two parameters would require additional measurements capturing the distribution of bacteria throughout space and orientation.

Our model and experiments have differences, such as assuming the two phases form a lamellar pattern with a flat interface. As seen in Fig. 1, the ATPS has a highly

curved interface, which can affect the distribution of bacteria. Moreover, the actual F_{max} that motile bacteria should overcome when crossing the interface is difficult to measure. In the optical tweezers experiment shown in Fig. 3A, the interface is easily deformed by the *B. subtilis*, which can drag the DEX-rich phase behind it when a bacterium passes through the interface. This deformation of the interface creates additional non-conservative interfacial tension-derived forces that are present in the measured F_{max} (See Fig. 3). However, the motile bacterium does not deform the interface that much when it crosses the interface by itself (see also Movie S1). This makes it challenging to find the exact chemical affinity of the bacteria to the DEX-rich domain. Finally, *B. subtilis* cells vary greatly in their body lengths, propulsive force, and tumbling rates; the bacteria propulsive force and the PEG-rich domain size heterogeneities are shown in Supplemental Fig. S6. This heterogeneity means that some bacteria are more likely to cross the interface than others, potentially enabling the ATPS to partition and sort the cells according to these properties. These factors will all increase the uncertainty of both the theoretical model and parameter estimation. Furthermore, as discussed earlier, while we do not expect the observed viscosity differences between the DEX-rich and PEG-rich regions to be large enough to explain the preferential partitioning present in our system, MIPS may contribute by slightly enhancing the partitioning effect as well.

In conclusion, we studied the competition between motility and two-phase boundaries on the biased partitioning of motile *B. subtilis* using experiment and theory. The motility of *B. subtilis* helps to distribute the bacteria across both DEX-rich and PEG-rich phases by providing a large propulsive force, $F_{\text{prop}} \approx 10\text{pN}$, to overcome the maximum interfacial force. We found that the chemical affinity of the *B. subtilis* cell wall with the DEX-rich phase generates interfacial forces on the bacterium with magnitudes spanning from $F_{\text{max}} = 2\text{pN}$ to 10pN , depending on the dextran composition.

J.C. and J.J. acknowledge the financial support from the National Research Foundation of Korea under NRF-2020R1A4A1019140 and NRF-2021R1A2C101116312. K.H.C., K.J.M., and S.C.T. are supported by the Air Force Office of Scientific Research under award number FA9550-21-1-0287. K.J.M. is also supported by the National Science Foundation Graduate Research Fellowship under Grant No. 2139319. S.C.T. is also supported by the Packard Fellowship in Science and Engineering.

* Equal contribution

† stakatori@ucsb.edu

‡ jjeong@unist.ac.kr

- [1] T. Yoshizawa, R.-S. Nozawa, T. Z. Jia, T. Saio, and E. Mori, Biological phase separation: cell biology meets biophysics, *Biophysical reviews* **12**, 519 (2020).
- [2] M. Iqbal, Y. Tao, S. Xie, Y. Zhu, D. Chen, X. Wang, L. Huang, D. Peng, A. Sattar, M. A. B. Shabbir, *et al.*, Aqueous two-phase system (atps): an overview and advances in its applications, *Biological procedures online* **18**, 1 (2016).
- [3] M. Dwidar, B. M. Leung, T. Yaguchi, S. Takayama, and R. J. Mitchell, Patterning bacterial communities on epithelial cells, *PLoS One* **8**, e67165 (2013).
- [4] P. Åke Albertsson, Partition of cell particles and macromolecules in polymer two-phase systems (Academic Press, 1970) pp. 309–341.
- [5] G. D. Baird, P. Åke Albertsson, and B. v. Hofsten, Separation of bacteria by counter-current distribution, *Nature* **192**, 236–239 (1961).
- [6] B. Hofsten, Partition of escherichia coli in an aqueous polymer two-phase system, *Experimental Cell Research* **41**, 117 (1966).
- [7] Q. Ma, Y. Song, W. Sun, J. Cao, H. Yuan, X. Wang, Y. Sun, and H. C. Shum, Cell-inspired all-aqueous microfluidics: from intracellular liquid–liquid phase separation toward advanced biomaterials, *Advanced Science* **7**, 1903359 (2020).
- [8] A. J. Huang, A. N. Clarke, N. Jafari, and B. M. Leung, Characterization of patterned microbial growth dynamics in aqueous two-phase polymer scaffolds, *ACS Biomaterials Science & Engineering* **7**, 5506 (2021).
- [9] H. Sakuta, T. Fujimoto, Y. Yamana, Y. Hoda, K. Tsumoto, and K. Yoshikawa, Aqueous/aqueous micro phase separation: construction of an artificial model of cellular assembly, *Frontiers in Chemistry* **7**, 44 (2019).
- [10] C. Shibata, K. Iwashita, and K. Shiraki, Salt-containing aqueous two-phase system shows predictable partition of proteins with surface amino acids residues, *International journal of biological macromolecules* **133**, 1182 (2019).
- [11] J. Kim, H. Shin, J. Kim, J. Kim, and J. Park, Isolation of high-purity extracellular vesicles by extracting proteins using aqueous two-phase system, *PloS one* **10**, e0129760 (2015).
- [12] W. Cui, C. Xia, S. Xu, X. Ye, Y. Wu, S. Cheng, R. Zhang, C. Zhang, and Z. Miao, Water-in-water emulsions stabilized by self-assembled chitosan colloidal particles, *Carbohydrate Polymers* **303**, 120466 (2023).
- [13] C. K. Byun, M. Kim, and D. Kim, Modulating the partitioning of microparticles in a polyethylene glycol (peg)-dextran (dex) aqueous biphasic system by surface modification, *Coatings* **8**, 85 (2018).
- [14] S. Singh and H. Tavana, Collagen partition in polymeric aqueous two-phase systems for tissue engineering, *Frontiers in Chemistry* **6**, 379 (2018).
- [15] M. Mastiani, N. Firoozi, N. Petrozzi, S. Seo, and M. Kim, Polymer-salt aqueous two-phase system (atps) microdroplets for cell encapsulation, *Scientific Reports* **9**, 15561 (2019).
- [16] M. E. Cates and J. Tailleur, Motility-induced phase separation, *Annual Review of Condensed Matter Physics* **6**, 219 (2015).
- [17] M. N. Van Der Linden, L. C. Alexander, D. G. Aarts, and O. Dauchot, Interrupted motility induced phase separation in aligning active colloids, *Physical review letters* **123**, 098001 (2019).
- [18] C. B. Caporusso, P. Digregorio, D. Levis, L. F. Cugliandolo, and G. Gonnella, Motility-induced microphase and macrophase separation in a two-dimensional active brownian particle system, *Physical Review Letters* **125**, 178004 (2020).
- [19] L. F. Garrity and G. W. Ordal, Chemotaxis in bacillus subtilis: How bacteria monitor environmental signals, *Pharmacology & Therapeutics* **68**, 87 (1995).
- [20] M. J. Tindall, P. K. Maini, S. L. Porter, and J. P. Armitage, Overview of mathematical approaches used to model bacterial chemotaxis ii: bacterial populations, *Bulletin of mathematical biology* **70**, 1570 (2008).
- [21] K. J. Modica and S. C. Takatori, Soft confinement of self-propelled rods: simulation and theory, *Soft Matter* **20**, 2331 (2024).
- [22] A. Baskaran and M. C. Marchetti, Hydrodynamics of self-propelled hard rods, *Phys. Rev. E* **77**, 011920 (2008).
- [23] J. Cheon, J. Son, S. Lim, Y. Jeong, J.-H. Park, R. J. Mitchell, J. U. Kim, and J. Jeong, Motile bacteria crossing liquid-liquid interfaces (2024), arXiv:2402.05095 [cond-mat.soft].